Solid-State Electronics xxx (2011) xxx–xxx

Contents lists available at SciVerse ScienceDirect

Solid-State Electronics

journal homepage: www.elsevier.com/locate/sse

Subband engineering in *n*-type silicon nanowires using strain and confinement

Zlatan Stanojević *, Viktor Sverdlov, Oskar Baumgartner, Hans Kosina

Institute for Microelectronics, TU Wien, Gußhausstraße 27–29, 1040 Wien, Austria

ARTICLE INFO

Article history:
Available online xxxx

Keywords:
Silicon nanowires
Strained silicon
Subband structure
Two-band **k** · **p** model
One-dimensional electron gas

ABSTRACT

We present a model based on **k** · **p** theory which is able to capture the subband structure effects present in ultra-thin strained silicon nanowires. For electrons, the effective mass and valley minima are calculated for different crystal orientations, thicknesses, and strains. The actual enhancement of the transport properties depends highly on the crystal orientation of the nanowire axis; for certain orientations strain and confinement can play together to give a significant increase of the electron mobility. We also show that the effects of both strain and confinement on mobility are generally more pronounced in nanowires than in thin films. We show that optimal transport properties can be expected to be achieved through a mix of confinement and strain. Our results are in good agreement with recent experimental findings.

1. Introduction and motivation

Nanowire-based gate-all-around transistors offer a perspective for further device size reduction in microelectronics. On one hand, gate-all-around device architectures exhibit superior electrostatic control of the channel over planar or silicon-on-insulator (SOI) technologies due to a high surface to volume ratio. Improved electrostatic control remedies short channel effects that plague modern planar technologies, especially in the subthreshold regime of operation. On the other hand, if the nanowire channels are made very thin, quantum effects begin to appear. While in traditional planar device architectures quantum effects almost always adversely affect device performance, they offer opportunities for performance improvement in non-planar architectures, such as transistors with nanowire channels.

In a recent experimental study [1], nanowires with gate-all-around structure as thin as 3 nm were successfully fabricated using a top down structuring process [2]. The produced nanowires had a [110] oriented axis and $(\bar{1}10)$ and (001) oriented walls. Most notably, the authors presented results of axially strained nanowire field effect transistors where the measured strain-induced current increase surpassed the current increase observed in (100) oriented thin SOI films in [110] direction by roughly a factor of two.

In this work we first attempt to examine in detail the subband structure effects causing the current enhancement. Then we explore the design space spanned by nanowire geometry (i.e. quantum confinement) and strain conditions. The outline of this paper is as follows: In Section 2 we will present the **k** · **p** model of the nanowire subband structure, which accurately treats confinement and strain. Here, we will also give some relevant details about the computational procedure itself. In Section 3 we will present the results of our subband structure calculations. Here, we will discuss the influence of nanowire diameter, cross-section shape, and stress on the subband structure and the transport properties arising therefrom. In Section 4 we will summarize and conclude this paper.

2. Subband structure modeling

To understand the transport properties in wires less than 10 nm wide, one must carefully take quantization effects into account. A simple treatment using effective masses fails to satisfactorily describe the subband structure of such thin devices. This is due to the energy of the lowest subband already being of the order of 100 meV where non-parabolicity effects become noticeable.

2.1. Bulk Hamiltonian

The starting point is the strain-dependent description of the bulk silicon conduction band structure using a two band **k** · **p** model which is due to Hensel et al. [3]. Commonly in **k** · **p** models, the expansion is taken around the Γ point where the minima and maxima of the interacting conduction and valence bands are located. This is practical for modeling band structures of direct semiconductors and in cases where one looks at the valence band structure only. In silicon, which has an indirect bandgap, this is not feasible. Therefore, the model used here assumes, that the interacting bands are the lowest two conduction bands, with the remaining bands being treated as perturbation. The expansion is performed around one of the three X points where a pair of adjacent Δ valleys touch.

* Corresponding author. Tel.: +43 1 58801 36016; fax: +43 1 58801 36099.
E-mail address: stanojevic@iue.tuwien.ac.at (Z. Stanojević).

0038-1101/$ - see front matter © 2011 Elsevier Ltd. All rights reserved.
doi:10.1016/j.sse.2011.11.022

The model is valid for the conduction band up to 0.5 eV, as was shown through benchmarking against density functional theory (DFT), semi-empirical tight binding (TB), and empirical pseudopotential method (EPM) calculations [4,5]. It includes a first-order treatment of uniaxial and shear strain effects on the conduction band by means of deformation potentials.

The model Hamiltonian describing a pair of adjacent Δ-valleys reads as follows:

$$\mathbf{H} = \begin{pmatrix} \frac{1}{2}\mathbf{p}^- \cdot \mathbf{m}^{-1} \cdot \mathbf{p}^- + \Xi_u \varepsilon_{\zeta\zeta} + V & -\frac{p_\xi p_\eta}{M} + 2\Xi_{u'}\varepsilon_{\xi\eta} \\ -\frac{p_\xi p_\eta}{M} + 2\Xi_{u'}\varepsilon_{\xi\eta} & \frac{1}{2}\mathbf{p}^+ \cdot \mathbf{m}^{-1} \cdot \mathbf{p}^+ + \Xi_u \varepsilon_{\zeta\zeta} + V \end{pmatrix} \quad (1)$$

$$\mathbf{p}^\pm = \hbar \begin{pmatrix} k_\xi \\ k_\eta \\ k_\zeta \end{pmatrix} \pm \hbar \begin{pmatrix} 0 \\ 0 \\ k_0 \end{pmatrix}, \quad \mathbf{m}^{-1} = \begin{pmatrix} m_t^{-1} & & \\ & m_t^{-1} & \\ & & m_l^{-1} \end{pmatrix}.$$

Here, $\mathbf{p}^\pm$ are the crystal momenta with respect to the valley minima. $\mathbf{m}^{-1}$ is the inverse of the effective mass tensor at each of the valley minima, with $m_l = 0.91 m_e$ and $m_t = 0.19 m_e$. $\frac{1}{M} \approx \frac{1}{m_t} - \frac{1}{m_e}$ describes the coupling between the two valleys; $k_0 = 0.15\frac{2\pi}{a}$ amounts to the distance in k-space between a X point and the Δ valley minima; $\varepsilon_{\zeta\zeta}$ and $\varepsilon_{\xi\eta}$ are uniaxial and shear strain components, and $\Xi_u = 9.0$ eV and $\Xi_{u'} = 7.0$ eV the respective deformation potentials. V denotes the conduction band edge.

The crystal momenta, k-vectors, masses, and strains in (1) are given in the coordinate system of the $\mathbf{k}\cdot\mathbf{p}$ expansion, $\mathbf{e}_\xi$, $\mathbf{e}_\eta$, $\mathbf{e}_\zeta$. One expansion gives a Hamiltonian for only two of the six conduction band valleys in silicon; the Hamiltonian for the other two valley pairs can be obtained by taking even permutations of the basis vectors. The device, which in our case is a nanowire channel, generally uses a coordinate system which differs from the one used in (1); we name it the device coordinate system $\mathbf{e}_x$, $\mathbf{e}_y$, $\mathbf{e}_z$, where $\mathbf{e}_z$ denotes the axial coordinate and $\mathbf{e}_x$ and $\mathbf{e}_y$ are the cross-section coordinates. The transformation matrix reads

$$\mathbf{U} = \begin{pmatrix} \mathbf{e}_\xi \cdot \mathbf{e}_x & \mathbf{e}_\xi \cdot \mathbf{e}_y & \mathbf{e}_\xi \cdot \mathbf{e}_z \\ \mathbf{e}_\eta \cdot \mathbf{e}_x & \mathbf{e}_\eta \cdot \mathbf{e}_y & \mathbf{e}_\eta \cdot \mathbf{e}_z \\ \mathbf{e}_\zeta \cdot \mathbf{e}_x & \mathbf{e}_\zeta \cdot \mathbf{e}_y & \mathbf{e}_\zeta \cdot \mathbf{e}_z \end{pmatrix}. \quad (2)$$

It is convenient to specify the device axes in terms of Miller indices. The main axis of our device is the nanowire axis, which can be specified e.g. as [1 1 0]. If we choose $\mathbf{e}_z$ as our nanowire axis, the third column in (2) becomes $(1\,1\,0)^T/\sqrt{2}$ in this case. If the wire is not rotationally symmetric the orientation of one of the surfaces must be specified additionally. Using the matrix from (2) we can establish the relations

$$\begin{pmatrix} k_\xi \\ k_\eta \\ k_\zeta \end{pmatrix} = \mathbf{U} \begin{pmatrix} k_x \\ k_y \\ k_z \end{pmatrix}, \quad \begin{pmatrix} k_\xi \\ k_\eta \\ k_\zeta \end{pmatrix}^T = \begin{pmatrix} k_x \\ k_y \\ k_z \end{pmatrix}^T \mathbf{U}^T. \quad (3)$$

Using these relations we can express the Hamiltonian (1) in terms of k_x, k_y, k_z, which are defined in the device coordinate system.

2.2. Quantization of the Hamiltonian

The next step is to introduce quantization. In a nanowire electrons are only partially quantized: while they are confined within the cross-section of the nanowire, they are free to move along the nanowire axis. This is modeled by substituting the k-vector components perpendicular to the axis with derivatives and by parametrizing the axial k-vector component.

$$k_x \mapsto -i\frac{\partial}{\partial x}, \quad k_y \mapsto -i\frac{\partial}{\partial y}, \quad k_z =: k_\parallel; \quad \mathbf{k}_q = \begin{pmatrix} -i\frac{\partial}{\partial x} \\ -i\frac{\partial}{\partial y} \\ k_\parallel \end{pmatrix} \quad (4)$$

The rotated Hamiltonian (1) can be expressed as

$$\mathbf{H} = \begin{pmatrix} \mathbf{k}_q^T \mathbf{D} \mathbf{k}_q & \mathbf{k}_q^T \mathbf{C} \mathbf{k}_q \\ \mathbf{k}_q^T \mathbf{C} \mathbf{k}_q & \mathbf{k}_q^T \mathbf{D} \mathbf{k}_q \end{pmatrix} + \begin{pmatrix} -\mathbf{d}^T \mathbf{k}_q & 0 \\ 0 & \mathbf{d}^T \mathbf{k}_q \end{pmatrix} + \begin{pmatrix} H_0^d & H_0^c \\ H_0^c & H_0^d \end{pmatrix}, \quad (5)$$

$$\mathbf{D} = \frac{\hbar^2}{2}\mathbf{U}^T \mathbf{m}^{-1} \mathbf{U}, \quad \mathbf{C} = -\frac{\hbar^2}{2M}\mathbf{U}^T \begin{pmatrix} 0 & 1 & 0 \\ 1 & 0 & 0 \\ 0 & 0 & 0 \end{pmatrix} \mathbf{U},$$

$$\mathbf{d} = \frac{\hbar^2}{m_l} \begin{pmatrix} 0 \\ 0 \\ k_0 \end{pmatrix} \mathbf{U}, \quad H_0^d = \frac{\hbar^2 k_0^2}{m_l} + \Xi_u \varepsilon_{\zeta\zeta} + V, \quad H_0^c = 2\Xi_{u'}\varepsilon_{\xi\eta}.$$

At this point the quantization is introduced by adding Dirichlet boundary conditions to the problem, i.e. we require the wavefunction to vanish at the nanowire boundary.

2.3. Stress and strain

Strain couples to the Hamiltonian through the deformation potentials Ξ_u and $\Xi_{u'}$. In the rotated Hamiltonian the contributions due to strain are summed up in the third term of (5). The relevant strain components $\varepsilon_{\xi\eta}$ and $\varepsilon_{\zeta\zeta}$ are given in the coordinate system of the $\mathbf{k}\cdot\mathbf{p}$ expansion, $\mathbf{e}_\xi$, $\mathbf{e}_\eta$, $\mathbf{e}_\zeta$, and are related to the stress tensor σ via the stiffness tensor,

$$\sigma = C\varepsilon, \quad \sigma_{ij} = C_{ijkl}\varepsilon_{kl}, \quad i,j,k,l \in \{\xi,\eta,\zeta\}, \quad (6)$$

which for silicon reads (in engineering notation)

$$C = \begin{pmatrix} C_{11} & C_{12} & C_{12} & & & \\ C_{12} & C_{11} & C_{12} & & & \\ C_{12} & C_{12} & C_{11} & & & \\ & & & C_{44} & & \\ & & & & C_{44} & \\ & & & & & C_{44} \end{pmatrix}, \quad (7)$$

$C_{11} = 166.0$ GPa, $C_{12} = 64.0$ GPa, $C_{44} = 79.6$ GPa [6].

Note, that the strains $\varepsilon_{\xi\eta}$ and $\varepsilon_{\zeta\zeta}$ influence only one of the three valley pairs. Since the Hamiltonians for the other two valley pairs are obtained by rotating the basis vectors, the basis of the strain tensors is rotated as well. Therefore, the relevant strain components for the other two valley pairs are $\varepsilon_{\eta\zeta}$, $\varepsilon_{\xi\xi}$ and $\varepsilon_{\xi\zeta}$, $\varepsilon_{\eta\eta}$, respectively.

In this work we are mainly interested in axial stresses in nanowires. The stress is therefore conveniently given as the stress scalar along the nanowire axis, $\sigma_\parallel$. The stress tensor in the crystallographic coordinate system of the $\mathbf{k}\cdot\mathbf{p}$ expansion is constructed as

$$\sigma = \mathbf{U} \begin{pmatrix} 0 & 0 & 0 \\ 0 & 0 & 0 \\ 0 & 0 & \sigma_\parallel \end{pmatrix} \mathbf{U}^T. \quad (8)$$

From this the strain tensor is obtained by using (6).

2.4. Discretization and numerical solution

The Hamiltonian now has to be discretized in two dimensions (x and y) using an appropriate discretization scheme. In this work we chose box integration because it inherently ensures probability current conservation which is crucial when simulating quantum mechanical systems. It should be noted that the different parts of (5) contribute derivatives of first and second order as well as constant terms. Looking at the symmetric matrices $\mathbf{D}$, $\mathbf{C}$ and the vector $\mathbf{d}$

$$\mathbf{D} = \left(\begin{array}{cc:c} D_{xx} & D_{xy} & D_{xz} \\ D_{yx} & D_{yy} & D_{yz} \\ \hdashline D_{zx} & D_{zy} & D_{zz} \end{array}\right), \quad \mathbf{C} = \left(\begin{array}{cc:c} C_{xx} & C_{xy} & C_{xz} \\ C_{yx} & C_{yy} & C_{yz} \\ \hdashline C_{zx} & C_{zy} & C_{zz} \end{array}\right), \quad \mathbf{d} = \left(\begin{array}{c} d_x \\ d_y \\ \hdashline d_z \end{array}\right), \quad (9)$$

Please cite this article in press as: Stanojević Z et al. Subband engineering in n-type silicon nanowires using strain and confinement. Solid State Electron (2011), doi:10.1016/j.sse.2011.11.022

we note that the coefficients marked by a solid line are from second order contributions and the coefficients marked by a dashed line are from first order contributions; D_{zz}, C_{zz}, and d_z are due to constant terms.

For each value of the $k_\parallel$-parameter, discretizing the Hamiltonian produces a system matrix **A**, the eigenvalues of which are the energies of the subband structure at this particular $k_\parallel$ value. To obtain a good approximation of the subband structure the Hamiltonian is discretized for a few hundred values of $k_\parallel$. The tasks of diagonalizing the Hamiltonian for different $k_\parallel$ values are mutually independent and can therefore be parallelized easily. An example of a calculated subband structure can be seen in Figs. 1 and 2.

Since we are interested in subbands within the energy range of several k_BT above the valley minimum, computational speed can be further improved if we restrict the calculation of the eigenenergies to the lowest few subbands. The implicitly restarted Arnoldi method (IRAM) provided by the ARPACK library [7] makes use of this restriction and gives sufficiently short computation times to allow the efficient simulation of nanowires up to 7 nm diameter. For larger diameters the energy spacing between the subbands becomes so small that an energy interval of a few k_BT may already contain hundreds of subbands. On the one hand, including more subbands results in a higher computational effort per Arnoldi iteration. On the other hand, closer spaced eigenvalues have a negative impact on convergence speed resulting in more Arnoldi iterations required to find them. This problem can be resolved using a spectral transformation on the matrix called shift-invert [7]. Here a diagonally shifted version of the original system matrix **A** needs to be factorized, i.e. the system

$$(\mathbf{A} - \sigma\mathbf{I})\mathbf{x} = \mathbf{b} \tag{10}$$

needs to be solved for different vectors **b** supplied by the IRAM procedure. The shift-invert transform increases the spacing between the eigenvalues and thus reduces the number required Arnoldi iterations. Also, using multiple shift-invert transformations the total number of subbands to be calculated can be split in several blocks where the number of subbands can be kept low enough for efficient calculation (about twenty subbands per block). The overall computation time then scales linearly with the total number of subbands. This allows us to simulate nanowires with 10 nm diameter and beyond.

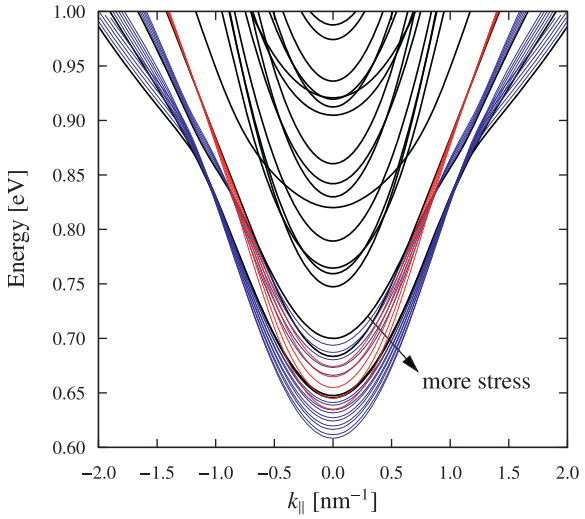

Fig. 1. Unprimed subbands in a [1 1 0] nanowire; black lines – unstrained, colored lines – tensile axial stresses up to 1 GPa (shown for the four lowest subbands only). (For interpretation of the references to colour in this figure legend, the reader is referred to the web version of this article.)

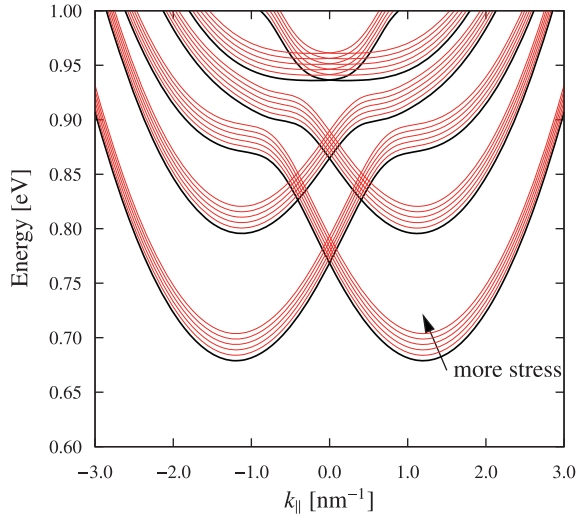

Fig. 2. Primed subbands in a [1 1 0] nanowire; black lines – unstrained, red lines – tensile axial stresses up to 1 GPa; plot is centered around the *X* point at the edge of the Brillouin zone. (For interpretation of the references to colour in this figure legend, the reader is referred to the web version of this article.)

2.5. Group velocity and effective mass – postprocessing

In the final step we need to extract macroscopically relevant quantities from the subband structure. These are the group velocities and effective masses of the confined electrons, which are related to the subband structure through the first and second derivatives with respect to $k_\parallel$.

In principle it would be possible to calculate the velocities and effective masses by numerical differentiation, i.e. by finite differences. However, this is not particularly advisable because a subband tends to warp significantly especially when energetically close to another subband. A finite difference scheme would require a very fine $k_\parallel$-grid for a reasonably accurate result, especially for the second order derivative.

There is a simple solution to this problem: The group velocity can be calculated using a technique derived from perturbation theory. From there, the effective mass can then be calculated by first order finite differences with satisfactory accuracy. We shall briefly explain the procedure of group velocity calculation in the following.

Non-degenerate perturbation theory states that in presence of a small perturbation δH the eigenenergy of a state will change according to

$$\delta E_i = \langle\psi_i|\delta H|\psi_i\rangle + \sum_{j\neq i} \frac{|\langle\psi_i|\delta H|\psi_j\rangle|^2}{E_i - E_j} + \mathcal{O}(\|\delta H\|^3). \tag{11}$$

We assume δH as the difference in the Hamiltonian between some points ${k_\parallel}^0$ and ${k_\parallel}^0 + \delta k_\parallel$ and approximate it using the $k_\parallel$-derivative of the Hamiltonian to get

$$\delta E_i \approx \left\langle \psi_i \left| \frac{\partial H}{\partial k_\parallel} \right| \psi_i \right\rangle \delta k_\parallel, \tag{12}$$

and obtain the derivative of the eigenenergy,

$$\frac{\partial E}{\partial k_\parallel} = \hbar v_g = \left\langle \psi_i \left| \frac{\partial H}{\partial k_\parallel} \right| \psi_i \right\rangle. \tag{13}$$

One could now proceed to obtain the second derivative by including the second order term in (11). This is impractical, however, because calculating the second order term would require all

Please cite this article in press as: Stanojević Z et al. Subband engineering in *n*-type silicon nanowires using strain and confinement. Solid State Electron (2011), doi:10.1016/j.sse.2011.11.022

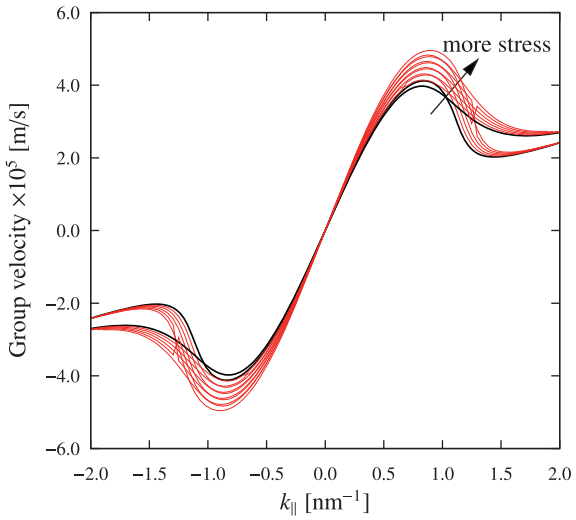

Fig. 3. Electron group velocities of the two lowest subbands in a [1 1 0] nanowire (see Fig. 1); black lines – unstrained, red lines – tensile axial stresses up to 1 GPa. (For interpretation of the references to colour in this figure legend, the reader is referred to the web version of this article.)

the matrix elements, or a sufficiently large number of them to keep the error low, whereas the first derivative needs only the diagonal matrix elements, resulting in a much lower computational effort.

In the case of degeneracies in the subband structure the degenerate perturbation theory must be employed. Here we need to distinguish between subbands which are degenerate everywhere, i.e. for all $k_\parallel$, and subbands which are degenerate only on a finite set of $k_\parallel$-points. For the former (13) still holds because moving along $k_\parallel$ does not lift the degeneracy and therefore $\langle\psi_i|\partial H/\partial\, k_\parallel|\psi_j\rangle$ vanishes for two degenerate subbands i and j. For the latter this is not the case and they need to be treated fully within the degenerate perturbation theory framework.

To obtain the matrix elements we need to calculate the operator $\partial H/\partial k_\parallel$. This is done by analytically differentiating the transformed Hamiltonian (5) with respect to $k_\parallel$ or k_z. This gives the matrix

$$\frac{\partial}{\partial k_\parallel}\mathbf{H} = \begin{pmatrix} \frac{\partial}{\partial k_z}\mathbf{k}_\mathrm{q}^T\mathbf{D}\mathbf{k}_\mathrm{q} & \frac{\partial}{\partial k_z}\mathbf{k}_\mathrm{q}^T\mathbf{C}\mathbf{k}_\mathrm{q} \\ \frac{\partial}{\partial k_z}\mathbf{k}_\mathrm{q}^T\mathbf{C}\mathbf{k}_\mathrm{q} & \frac{\partial}{\partial k_z}\mathbf{k}_\mathrm{q}^T\mathbf{D}\mathbf{k}_\mathrm{q} \end{pmatrix} + \begin{pmatrix} -d_z & 0 \\ 0 & d_z \end{pmatrix}. \tag{14}$$

Using (9) the elements in (14) evaluate to

$$\frac{\partial}{\partial k_\parallel}\mathbf{k}_\mathrm{q}^T\mathbf{D}\mathbf{k}_\mathrm{q} = 2D_{xz}\left(-i\frac{\partial}{\partial x}\right) + 2D_{yz}\left(-i\frac{\partial}{\partial y}\right) + 2D_{zz}k_\parallel, \tag{15}$$

$$\frac{\partial}{\partial k_\parallel}\mathbf{k}_\mathrm{q}^T\mathbf{C}\mathbf{k}_\mathrm{q} = 2C_{xz}\left(-i\frac{\partial}{\partial x}\right) + 2C_{yz}\left(-i\frac{\partial}{\partial y}\right) + 2C_{zz}k_\parallel, \tag{16}$$

The matrix elements are calculated by numerically computing the integrals

$$\left\langle\psi_i\left|\frac{\partial H}{\partial k_\parallel}\right|\psi_i\right\rangle = \int\left(\psi_i^{1*}\psi_i^{2*}\right)\frac{\partial}{\partial k_\parallel}\mathbf{H}\begin{pmatrix}\psi_i^1\\ \psi_i^2\end{pmatrix}\mathrm{d}A, \tag{17}$$

where the superscript in ψ_i^1 and ψ_i^2 denotes the index of the bulk band. An example of group velocities calculated using this method can be seen in Fig. 3.

3. Results and discussion

Using the model and procedure described in the previous section, we simulated nanowires of various diameters assuming square and rectangular cross-sections. The effect of axial stress on the subband structure was mainly investigated in this work. Axial tensile stress is the most likely type of stress to be implemented in a top-down nanowire process, as was demonstrated in [1], and is also a promising technique for mobility enhancement.

Self-consistency was not considered in this work, since we are attempting to isolate the effects of confinement and strain on the subband structure. A positive gate bias would increase the splitting between the unprimed and primed valleys for nanowires thicker than 5 nm. This effect was already studied elsewhere [8] and is beyond the scope of this paper.

3.1. Stress behavior of [1 1 0] and [1 1 1] nanowires

Fig. 1 shows the unprimed subbands of a [1 1 0] oriented 5 nm square nanowire. The shape of the subbands is highly non-parabolic which clearly justifies the use of band structure modeling methods beyond the effective mass approximation, such as $\mathbf{k}\cdot\mathbf{p}$. Fig. 2 shows the primed subbands, which are due to valleys that have a lighter quantization mass and therefore lie higher in energy than the unprimed ones. Note, that for [1 1 0] oriented nanowires confinement causes the unprimed subband minima to be folded onto $k_\parallel = 0$, i.e. the Γ point of the one-dimensional Brillouin zone. We shall, therefore, refer to these subbands also as Γ valley.

In both figures the colored lines show the trend of the subband structure change as tensile stress increases up to 1 GPa. The unprimed subbands in Fig. 1 have their valley minima shifted downwards in energy while at the same time their curvature increases. Therefore, we can expect a significant effective mass reduction in the unprimed subbands. In the primed subbands (Fig. 2) tensile stress induces only an upward shift but no change in curvature.

Fig. 4 shows the overall behavior of the confined electrons' effective mass as a function of axial stress for various nanowire thicknesses. We note that both confinement and tensile stress reduces the unprimed subbands' effective mass. Both, however, act in a competitive way: An already low effective mass, due to confinement, undergoes a much smaller change when the nanowire is stressed. For a 12 nm nanowire an axial stress of 1 GPa causes a 22.2% reduction of the effective mass, while in a 3 nm nanowire only 12.2% can be observed. Confinement and [1 1 0] stress both increase the off-diagonal part of the Hamiltonian (1) which explains the competitiveness. As can be seen for all curves in Fig. 4, the impact on the effective mass saturates for high tensile stresses. This saturation effect was already observed in ultra-thin films from calculations using the same model [9]. Apparently the onset of the

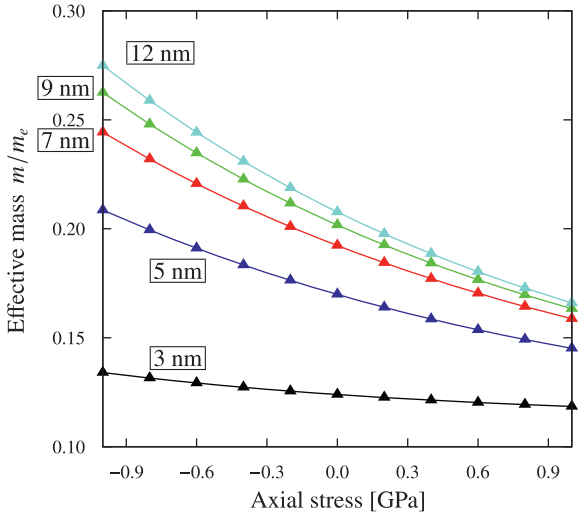

Fig. 4. Stress dependence of the effective mass in the unprimed (Γ) valley for [1 1 0] nanowires of different thicknesses.

Please cite this article in press as: Stanojević Z et al. Subband engineering in *n*-type silicon nanowires using strain and confinement. Solid State Electron (2011), doi:10.1016/j.sse.2011.11.022

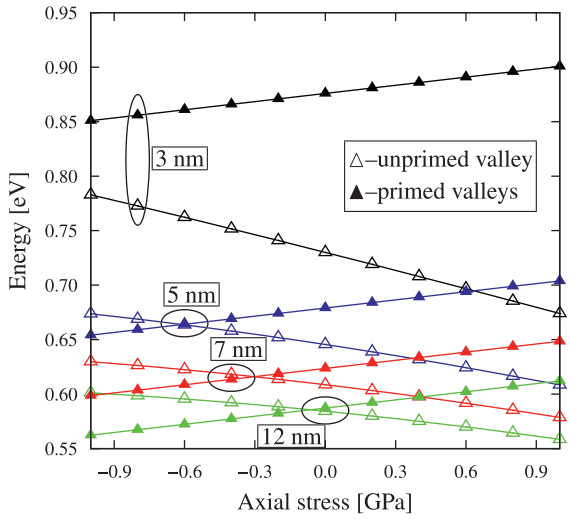

Fig. 5. Energy of valley minima for varying axial stress and different thicknesses of [1 1 0] nanowires.

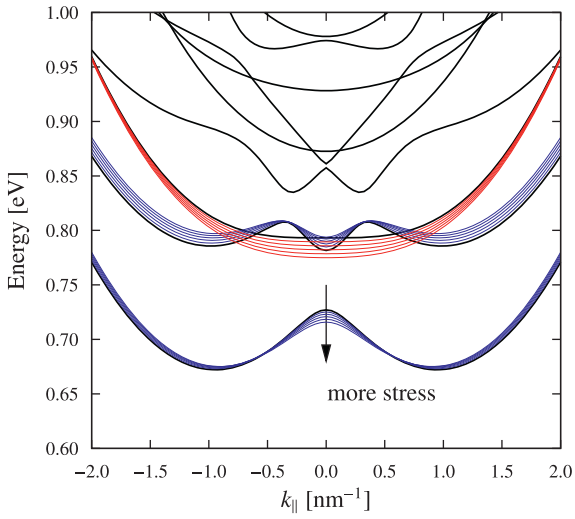

Fig. 7. Same as Fig. 1 for a [1 1 1] nanowire; black lines – unstrained, colored lines – tensile axial stresses up to 1 GPa (shown for the three lowest subbands only). (For interpretation of the references to colour in this figure legend, the reader is referred to the web version of this article.)

saturation occurs at lower stresses for smaller diameters due to quantization.

In Fig. 5 the behavior of the valley minima with respect to axial stress is shown. The unprimed and primed valleys shift in energetically opposite directions when stress is applied, as already mentioned. In this context, tensile stress also benefits the transport properties because it causes a separation of the light unprimed and the heavy primed subbands which effects a higher electron population in the light subbands (see Fig. 6) and a lower intervalley scattering rate due to the energetic remoteness of the primed subbands. We note that for the 3 nm nanowire the unprimed and primed subbands are already far apart due to confinement, so strain will cause no significant improvement, while for the 12 nm nanowire the subband minima almost coincide in energy, which makes application of stress mandatory in order to observe any mobility enhancement.

The situation is entirely different for [1 1 1] nanowires. Here, all valleys have the same quantization mass, and thus no distinction between unprimed and primed subbands is made. As can be seen in Fig. 7, the axial stress merely deforms the subbands without causing any significant shifts or curvature changes in the subband minima. Both confinement and tensile stress cause a splitting of the subbands a the Γ point; the splitting between the first and second subband eventually becomes so large that the two minima merge into a single heavy-effective-mass minimum; this indeed happens for the 3 nm nanowire. The simulation results presented in Figs. 8 and 9 confirm that axial stress is not beneficial for transport properties in [1 1 1] nanowires.

3.2. Influence of the aspect ratio on stress behavior

We will now assume the cross-section shape of the nanowires to be rectangular and look at the influence of the rectangle's aspect ratio on the subband structure. We performed several simulations on *n*-type nanowires of rectangular cross-section while varying the width of the cross-section from 5 nm to 15 nm and keeping the height at 5 nm, similar to recent studies performed for *p*-type nanowires [10,11]. Two sets of simulations were performed assuming the varied surfaces to be $(\bar{1}10)$-oriented in one case and (001)-oriented in the other. Both sets of simulations showed

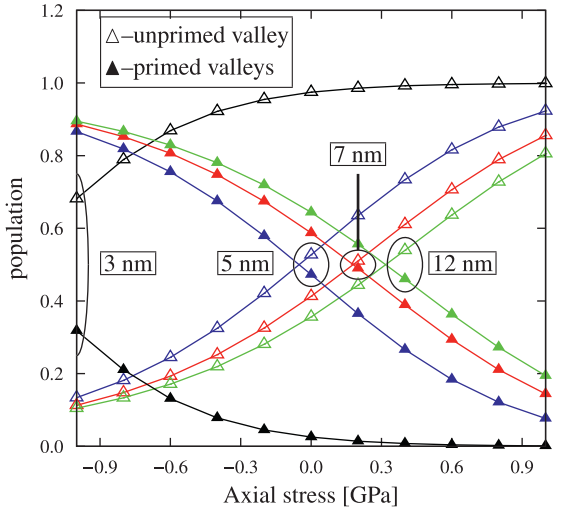

Fig. 6. Relative population of unprimed and primed valleys for varying axial stress and different thicknesses of [1 1 0] nanowires.

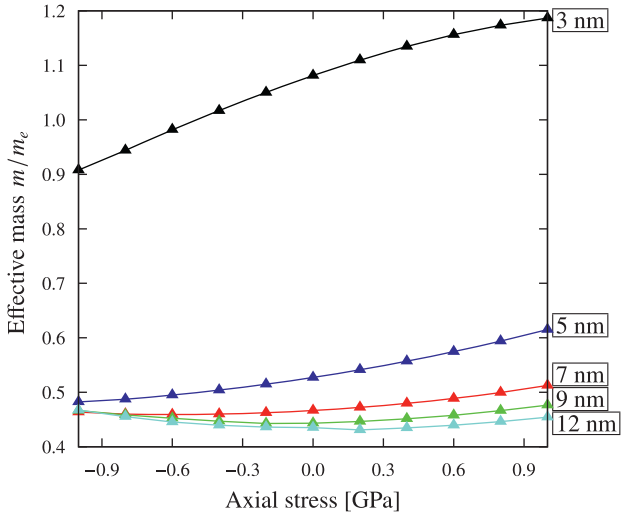

Fig. 8. Stress dependence of the effective mass for [1 1 1] nanowires of different thicknesses.

Please cite this article in press as: Stanojević Z et al. Subband engineering in *n*-type silicon nanowires using strain and confinement. Solid State Electron (2011), doi:10.1016/j.sse.2011.11.022

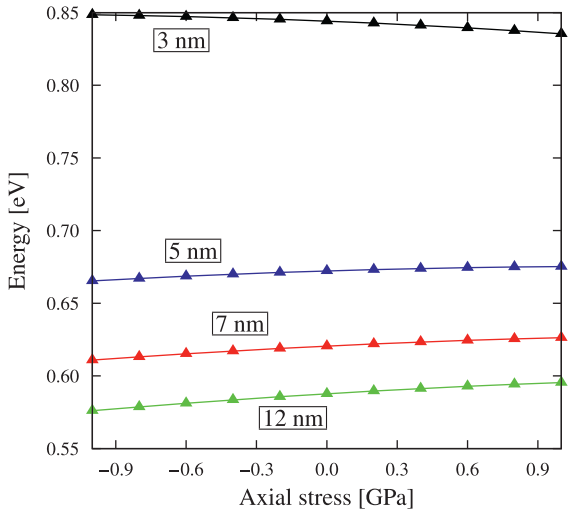

Fig. 9. Energy of valley minima for varying axial stress and different thicknesses of [1 1 1] nanowires.

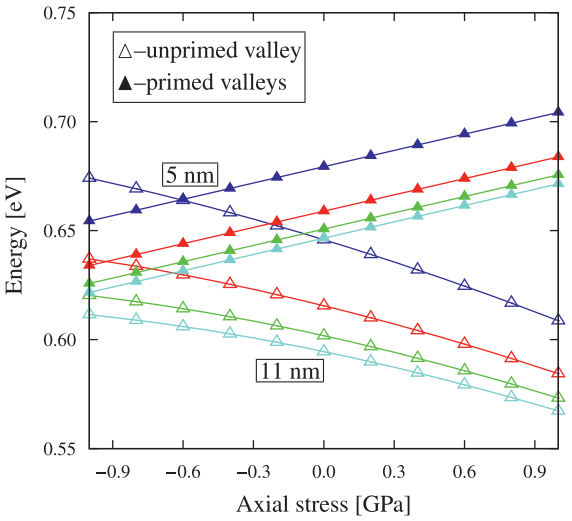

Fig. 11. Energy of valley minima of [1 1 0] nanowires for varying axial stress and different widths along [$\bar{1}$ 1 0].

significantly different results, which points out the strong influence of the cross-section shape on the transport properties.

In Figs. 10 and 11 the stress dependence of the effective mass and valley minima is shown for different widths along the [$\bar{1}$ 1 0] axis. The confinement width along [$\bar{1}$ 1 0] clearly affects the effective mass and the influence of axial stress upon it. This stems from the fact that by changing the width along any of the ⟨1 1 0⟩ axes one changes the quantization of the off-diagonal coupling elements in (1); these elements are responsible for all the observed effective mass variations. The valley minima also change with the width variation; interestingly, the separation between the unprimed and primed valleys becomes larger as the width increases.

In contrast, Fig. 12 shows no change of the effective mass or its stress dependence when the width is changed along [0 0 1]. Since for the Γ valley the width change along [0 0 1] changes the quantization only along the ζ axis in the Hamiltonian (1). The coupling elements and therefore the effective mass remain almost unaffected. The valley minima still respond to the width variations (Fig. 13) but in a different way from what could be seen in

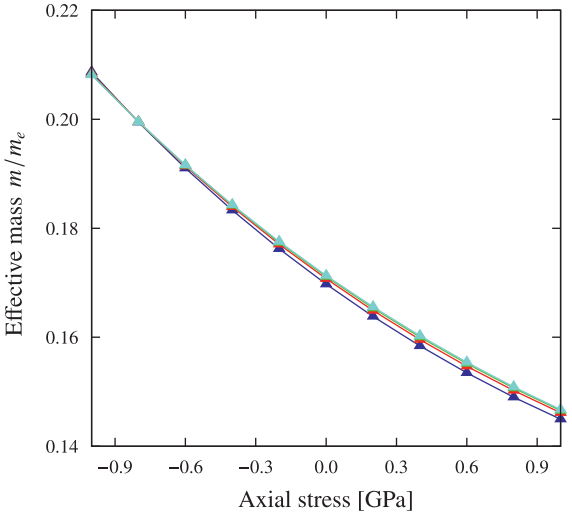

Fig. 12. Same as in Fig. 10 but for varying widths along [0 0 1]; here, the curves are on top of each other indicating that confinement along [0 0 1] has no influence on the effective mass in the unprimed valley.

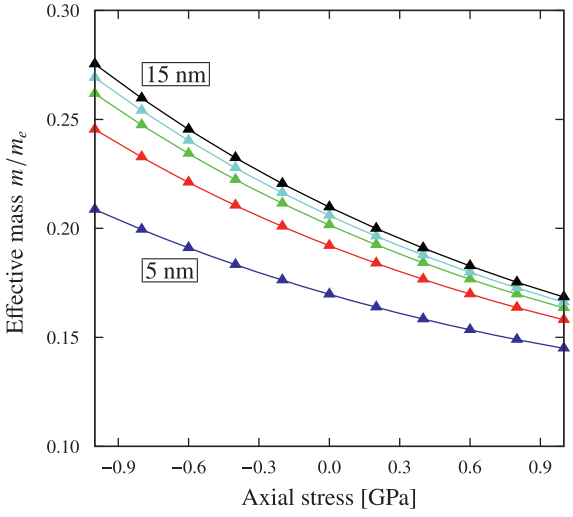

Fig. 10. Stress dependence of the effective mass in the unprimed (Γ) valley in [1 1 0] slabs of different widths along [$\bar{1}$ 1 0]; widths: 5 nm, 7 nm, 9 nm, 11 nm; height: 5 nm; changing the slab thickness along [$\bar{1}$ 1 0] clearly affects the effective mass and its dependence on axial strain.

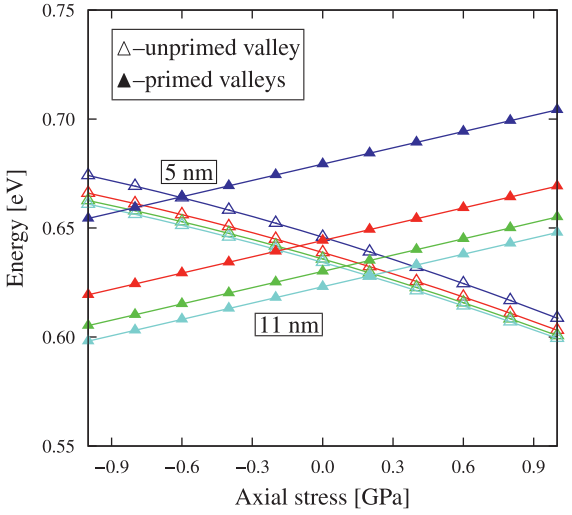

Fig. 13. Energy of valley minima of [1 1 0] nanowires for varying axial stress and different widths along [0 0 1].

Please cite this article in press as: Stanojević Z et al. Subband engineering in *n*-type silicon nanowires using strain and confinement. Solid State Electron (2011), doi:10.1016/j.sse.2011.11.022

Fig. 11; here, the separation between unprimed and primed valleys decreases as the width increases, and for large diameters the primed bands move below the unprimed in the unstrained state.

This lets us conclude that the cross-section shape of [110] nanowire can be used as an additional design parameter to tune the transport characteristics of nanowires. The dimensions along $[\bar{1}10]$ and [001] affect the subband structure in fundamentally different ways. While confinement along $[\bar{1}10]$ lets us adjust the effective mass of the confined electrons, the confinement along [001] allows us to define the energy separation between the unprimed and primed valleys as well as among the subbands within a particular valley, without affecting the transport mass. Therefore, a device optimized for high currents would have a narrow [001] dimension to keep the subbands well separated and a moderate $[\bar{1}10]$ dimension which in combination with tensile axial stress will give a light transport mass.

3.3. Comparison of nanowires with thin films

In [1] the authors have found that the on-current increase with tensile stress in 11.2 nm [110] nanowire *n*-type FETs is about twice as large as for a comparable ultra-thin body (UTB) transistor. This can be attributed to electrons in a nanowire forming a one-dimensional electron gas, whereas in a UTB they form a two-dimensional electron gas. To explain this discrepancy we will employ a simple Drude model to estimate the drift movement of the electrons in nanowire and UTB channels.

$$\langle v\rangle = -\frac{q_0\langle\tau\rangle}{m_{\text{eff}}}\mathcal{E} \tag{18}$$

Here, $\langle v\rangle$ is the average electron velocity, q_0 is the elementary charge, $\langle\tau\rangle$ is the average momentum relaxation time, m_{eff} is the effective mass, and $\mathcal{E}$ is the electric field. The model is, of course, insufficient for an accurate description of the electron movement because it assumes a single parabolic (sub)band. However, the main point here is the dependence of $\langle\tau\rangle$ on the effective mass. In a one-dimensional system the density-of-states mass is the same as the transport mass m_{eff}. If we change the effective mass through confinement or mechanical stress, the electrons both become lighter and scatter less often, since $\tau(E)$ is inversely proportional to the density of states $g(E)$ which for one-dimensional systems is proportional to $\sqrt{m_{\text{eff}}}$, hence $\langle\tau\rangle \propto m_{\text{eff}}^{-1/2}$ and $\langle v\rangle \propto m_{\text{eff}}^{-3/2}$. Indeed, inserting our calculated masses for the 12 nm [110] nanowire gives a velocity enhancement of 27.4% which agrees very well with the 30% found experimentally [1].

In two-dimensional systems the simple relation derived before does not hold because m_{eff} and m_{dos}, the density-of-states mass, are not equal. The density-of-states mass takes the transverse mass into account, which for thin silicon films in [110] direction is increased by tensile strain, as shown in [9]. The effect of strain on the masses cancels out in the average free flight time and $\langle v\rangle \propto m_{\text{eff}}^{-1}$ resulting in a lower current enhancement due to stress.

4. Summary and conclusions

In this work we have used a two band $\mathbf{k}\cdot\mathbf{p}$ model for the conduction band of bulk silicon and adapted it for *n*-type silicon nanowires. The model provides us with an accurate description of non-parabolicity in the silicon conduction band and includes a treatment of strain effects on the band structure. In the course of the work we have also developed computational methods for dealing with a large number of medium to large-scale eigenvalue problems, i.e. the calculation of the subband structure. The necessary algorithms were implemented within the Vienna Schrödinger Poisson solver framework [12], and allow all the calculations performed in this paper to be executed on a common workstation computer. Furthermore, a method was presented to obtain the exact value of the group velocities at a certain point in *k*-space without numerical differentiation of the subband structure. Skipping one numerical differentiation step improves the accuracy of the effective mass extraction from the subband structure. Its usability is not restricted to our calculations but can be used in other $\mathbf{k}\cdot\mathbf{p}$ models and can in principle be extended to any (sub)band structure calculation method relying on the repeated diagonalization of a *k*-dependent Hamiltonian, such as tight binding or pseudopotential methods.

With the presented simulation framework we have studied the behavior of axially stressed silicon nanowires of various thicknesses. We have shown how confinement and stress act on the electron subband structure of nanowires and pointed out where performance improvement can be expected. The effect of different aspect ratios of the nanowire cross-section on the subband structure properties was investigated for [110] nanowires. It was found that confinement along the $[\bar{1}10]$ and [001] axes has profoundly different effects on the subband structure. It was made clear that diameter, cross-section shape, and stress offer an additional design space for future devices based on [110] nanowire channels. This allows tuning the device for a particular application through geometrical patterning and application of stress during the fabrication process.

Finally, we addressed the question why the measured current enhancement of stressed nanowires is significantly larger than in thin films under the same stress conditions [1]. According to our results, the effect can be attributed to the one-dimensional nature of the electrons confined in a nanowire. Using a simple transport model for the confined electrons we calculated a stress-induced current enhancement figure close to the one obtained experimentally.

Acknowledgment

This work has been supported by the Austrian Science Fund, special research program IR-ON (F2509).

References

[1] Bangsaruntip S, Majumdar A, Cohen G, Engelmann S, Zhang Y, Guillorn M, et al. Gate-all-around silicon nanowire 25-stage CMOS ring oscillators with diameter down to 3 nm. In: Symposium on VLSI technology, 2010 (VLSIT, 2010); 2010. p. 21–2. doi:10.1109/VLSIT.2010.5556136.

[2] Bangsaruntip S, Cohen G, Majumdar A, Zhang Y, Engelmann S, Fuller N, et al. High performance and highly uniform gate-all-around silicon nanowire MOSFETs with wire size dependent scaling. In: IEEE international electron devices meeting (IEDM, 2009); 2009. p. 1–4. doi:10.1109/IEDM.2009.5424364.

[3] Hensel JC, Hasegawa H, Nakayama M. Cyclotron resonance in uniaxially stressed silicon. II: nature of the covalent bond. Phys Rev 1965;138(1A):A225–38. doi:10.1103/PhysRev.138.A225.

[4] Sverdlov V, Karlowatz G, Dhar S, Kosina H, Selberherr S. Two-band $\mathbf{k}\cdot p$ model for the conduction band in silicon: impact of strain and confinement on band structure and mobility. Solid-State Electron 2008;52(10):1563–8.

[5] Sverdlov VA, Windbacher T, Schanovsky F, Selberherr S. Mobility modeling in advanced MOSFETs with ultra-thin silicon body under stress. J Integr Circ Syst 2009;4(2):55–60.

[6] Levinstein M, Rumyantsev S, Shur M. Handbook series on semiconductor parameters. London: World Scientific; 1996. vol. 1. 2, 1999, 191.

[7] Lehoucq R, Sorensen D, Yang C. ARPACK users' guide: solution of large-scale eigenvalue problems with implicitly restarted arnoldi methods; 1998.

[8] Neophytou N, Paul A, Lundstrom MS, Klimeck G. Self-consistent simulations of nanowire transistors using atomistic basis sets. In: Grasser T, Selberherr S, editors. Simulation of semiconductor processes and devices 2007. Vienna: Springer; 2007. p. 217–20. doi:10.1007/978-3-211-72861-1_51, URL http://dx.doi.org/10.1007/978-3-211-72861-1_51.

[9] Sverdlov V, Baumgartner O, Windbacher T, Schanovsky F, Selberherr S. Thickness dependence of the effective masses in a strained thin silicon film. In: International conference on Simulation of semiconductor processes and devices, 2009 (SISPAD '09); 2009. p. 1–4. doi:10.1109/SISPAD.2009.5290252.

[10] Neophytou N, Kosina H. Large enhancement in hole velocity and mobility in *p*-type [110] and [111] silicon nanowires by cross section scaling: an atomistic analysis. Nano Lett 2010;10(12):4913–9. doi:10.1021/nl102875k, http://dx.doi.org/10.1021/nl102875k.

[11] Neophytou N, Klimeck G, Kosina H. Subband engineering for *p*-type silicon ultra-thin layers for increased carrier velocities: an atomistic analysis. J Appl Phys 2011;109(5):053721. doi:10.1063/1.3556435.

[12] Karner M, Gehring A, Holzer S, Pourfath M, Wagner M, Goes W, et al. A multi-purpose Schrödinger–Poisson solver for TCAD applications. J Comput Electron 2007;6(1):179–82.

Please cite this article in press as: Stanojević Z et al. Subband engineering in *n*-type silicon nanowires using strain and confinement. Solid State Electron (2011), doi:10.1016/j.sse.2011.11.022